

Preparation of Ni-Zn-doped porous carbon materials (Ni@C) as electrochemical sensor for hydroquinone detection

Yuxi Yang

Jingdezhen Vocational University of Art, Jingdezhen 333000, China

E-mail: 785348913@qq.com

Received: 4 July 2022 / Accepted: 2 August 2022 / Published: 10 September 2022

In this work, Ni-Zn-doped porous carbon materials (Ni@C) with regular dodecahedral morphologies were synthesized by calcination of Ni-doped ZIF-8 as a template, and applied in electrochemical sensing and quantitative electrochemical sensors to detect Hydroquinone (HQ). The uniformly dispersed Ni in Ni@C serves as the catalytically active material, and the synergistic effect of elemental Zn and porous carbon improves the electron transport efficiency of the material. The developed Ni@C electrochemical sensor detected HQ alone with a sensitivity of $180 \mu\text{A} \mu\text{M}^{-1} \text{cm}^{-2}$ and a linear range of 9.1 nM-80 μM . The results demonstrate that the enzyme-free electrochemical sensor based on Ni@C/GCE exhibits good sensitivity, a wide linear range and excellent selectivity. At the same time, the problem of the general conductivity of metal-organic framework (MOF) materials is solved, which provides a new idea for the application of such new materials in the direction of electrochemistry.

Keywords: metal organic framework; hydroquinone; electrochemical sensor

1. INTRODUCTION

Among the existing analytical techniques, electrochemical sensors stand out due to their high sensitivity, fast detection, simple operation, and easy miniaturization. [1-2] Direct detection using common electrodes (such as carbon electrodes and metal electrodes) usually has problems, such as large overpotential, poor stability and low selectivity, so we need to develop electrode modification materials with excellent performance. Among the possibilities, surface and interface effects, small size effects, quantum size effects and macroscopic quantum tunneling effects endow metal nanoparticles (MNPs) with the advantages of large specific surface area, high specific surface energy, abundant active sites, good electrical conductivity and good catalytic performance, making MNPs excellent electrode modification materials. [3-4] However, the high surface area allows MNPs to easily agglomerate during the synthesis process, so the preparation of stable small MNPs will face greater challenges [5-7]. To address this problem, many materials with large surface areas (such as porous carbon, graphene, and

metal-organic frameworks) are often used as supporting matrices to prepare stably dispersed small MNPs. However, there is almost no force between these supporting matrices and MNPs, resulting in the easy shedding or aggregation of MNPs from the surface of these substrate materials. Therefore, exploring new support materials is of great significance to obtain monodisperse MNPs with good catalytic performance.

Metal-organic frameworks (MOFs) are porous functional polymers composed of organic ligands bound to metal ions through coordination. Compared with traditional porous materials, such as zeolites and porous oxides, MOFs exhibit many excellent properties, including intercross linked topology, uniform pore size, constructable functionalized framework, and ultrahigh specific surface area. [8-10] The MOF (DUT-60) reported by H \ddot{u} nicke's group has a specific surface area as high as 7840 m²/g. [11] Based on these characteristics, MOFs have been widely used in the fields of gas adsorption, biomedicine, sensing analysis, organocatalysis, and energy storage. In the past few years, MOFs have gradually become precursors and templates for the preparation of porous carbon structures and metal/carbon and carbon shell structures. Among these, the zeolite imidazolium framework (ZIF) is the most commonly used MOF precursor. The structure of ZIF is similar to the zeolite topology, so they combine the various advantages of MOFs and zeolites, for example, high specific surface area, good crystallinity and many other features, as well as excellent chemical and thermal stability. Among them, ZIF-8 is an excellent candidate for the formation of Zn-containing nanostructures and layered nanoporous carbons. First, a material combining a porous carbon substrate and metal nanoparticles can be provided by in situ carbonization. The synergistic effect of metal nanoparticles and porous carbon substrates can further enhance the electrocatalytic effect, and the in-situ preparation process is conducive to the formation of uniform embedding in the carbon framework. The mixed metal/metal oxide nanoparticles in the medium avoid the falling off or agglomeration of mixed metal oxides into larger particles. Second, the carbon matrix with a large specific surface area evenly disperses the active metal nanoparticles, exposing more active sites, giving the detection object, and the active material a larger active contact area. [12-14]

Hydroquinone (HQ, 1,4-dihydroxybenzene) is a phenolic compound that occurs naturally in wood, tobacco smoke, coal tar, crude oil, and other materials. [15-18] Due to its high toxicity and low degradability in the ecological environment, its presence in cosmetics, pharmaceuticals, the environment and the human diet cause environmental pollution and risks to human health. The U.S. The Environmental Protection Agency (EPA) and the European Union (EU) have included hydroquinone on their lists of priority pollutants. According to the Chinese National Standard (GB 8978-1996), the acceptable emission of phenolic compounds is 0.5 mg mL⁻¹.

To date, various detection methods have been established for the determination of HQ, such as capillary electrophoresis, fluorescence, gas chromatography (GC), spectrophotometry, and high-performance liquid chromatography (HPLC). Compared with electrochemical methods, they have the advantages of simple operation, fast response, and low cost, providing opportunities for portable, inexpensive and fast methods; thus, they have received extensive attention. Existing studies have found that the electrochemical detection of HQ with bare electrodes is not very effective, showing a high detection limit and low sensitivity because the oxidation of HQ on bare electrodes is very slow. To improve its electrochemical analysis, it is necessary to synthesize and select appropriate modified electrode materials.

Here, we propose a Zn-Ni-doped porous carbon material (Ni@C) with a Ni-doped ZIF-8 precursor. Ni in Ni@C improves the overall catalytic effect of the material, while the synergistic effect of Zn and porous carbon improves the electron transport efficiency of the material. Based on the above advantages, the composite material was used for the detection of HQ and showed an excellent catalytic effect, good stability and high selectivity.

2. EXPERIMENTAL

2.1 Reagents

All chemicals were obtained commercially and used without further purification. $\text{Zn}(\text{NO}_3)_2 \cdot 6\text{H}_2\text{O}$, $\text{Ni}(\text{NO}_3)_2 \cdot 6\text{H}_2\text{O}$, 2-methylimidazole reagent (HMeIM), glacial acetic acid ($\text{C}_2\text{H}_4\text{O}_2$), N,N-dimethylformamide (DMF), methanol (MeOH), and tetrahydrofuran were purchased from Aladdin Co., Ltd. (Shanghai, China). Disodium hydrogen phosphate, sodium dihydrogen phosphate, ethanol and other chemicals were purchased from Beijing Chemical Reagent Factory (Beijing, China). Phosphate buffered saline (0.2 M PBS) was made from a solution of 0.2 M disodium hydrogen phosphate and 0.2 M sodium dihydrogen phosphate. All reagents were of analytical grade.

2.2 Experimental procedures for materials

(1) Preparation of Ni^{2+} -ZIF-8: by stirring a mixture of $\text{Zn}(\text{NO}_3)_2 \cdot 6\text{H}_2\text{O}$ (3.3 mmol), $\text{Ni}(\text{NO}_3)_2 \cdot 6\text{H}_2\text{O}$ (1.3 mmol) and HMeIM (31.6 mmol) in methanol (120 mL) after 24 hours, a lavender sample was obtained. After washing 3 times with methanol (60 mL), the solution was centrifuged to dry it to obtain a purple powder, Ni^{2+} -ZIF-8.

(2) Preparation of Ni@C: In a hydrogen-argon-saturated atmosphere, the abovementioned Ni^{2+} -ZIF-8 was placed in a porcelain boat, placed in a tubular atmosphere furnace for calcination, and heated at 700 °C for 3 hours. Then, the temperature was increased at a rate of 5 °C·min⁻¹ to obtain Ni@C.

(3) Preparation of Ni@C/GCE, Ni^{2+} -ZIF-8/GCE, and GCE: 2 mg of Ni^{2+} -ZIF-8 and Ni@C were dispersed in 1 mL of ultrapure water with thorough sonication. The dispersions were dropped on the glassy carbon electrode surface that was cleaned by polishing to obtain Ni^{2+} -ZIF-8/GCE and Ni@C/GCE. The figure shows a schematic diagram of the preparation process of Ni@C and the reaction process on the electrode surface.

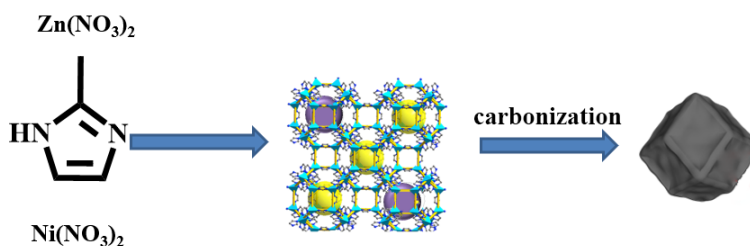


Figure 1. Schematic diagram

3. RESULTS AND DISCUSSION

3.1 Characterization of Ni²⁺-ZIF-8 and Ni@C

First, a nanoscale uniform Ni²⁺-ZIF-8 dodecahedral structure was synthesized by the coordination reaction between Zn(NO₃)₂•6H₂O, Ni(NO₃)₂•6H₂O and 2-methylimidazole. The rhombic dodecahedral morphology of Ni²⁺-ZIF-8 crystals is well constructed, with good polygonal morphology, a smooth surface and uniform particle size of approximately 20-50 nm. This indicates that doping a small amount of Ni into the framework of ZIF-8 does not change the unique morphological characteristics of ZIF-8. At the same time, nanoscale particles were synthesized by adjusting the concentration ratio of metal ions and dimethylimidazole, which would be more conducive to the exposure of the active sites of the material. Subsequently, the polyhedron was calcined at 700 °C under an argon flow to obtain Ni²⁺-ZIF-8-derived Ni@C, in which the organic linkages contained in Ni²⁺-ZIF-8 were carbonized into a carbon framework network, while Ni²⁺ was converted into Ni or its oxide form and doped into the framework. Figure 2A shows that Ni²⁺-ZIF-8 is a standard regular octahedron image, and Figure 2B shows a TEM image of Ni@C, which demonstrates that Ni@C does not change the morphology of the material much during the carbonization process. The nanoporous Ni@C particles show an uneven surface and a more transparent polyhedral structure, which is due to the decomposition and evaporation of some organic linkers in the form of small molecules such as water and carbon dioxide during the carbonization process. This hollow structure can provide a stable framework with a large specific surface area.

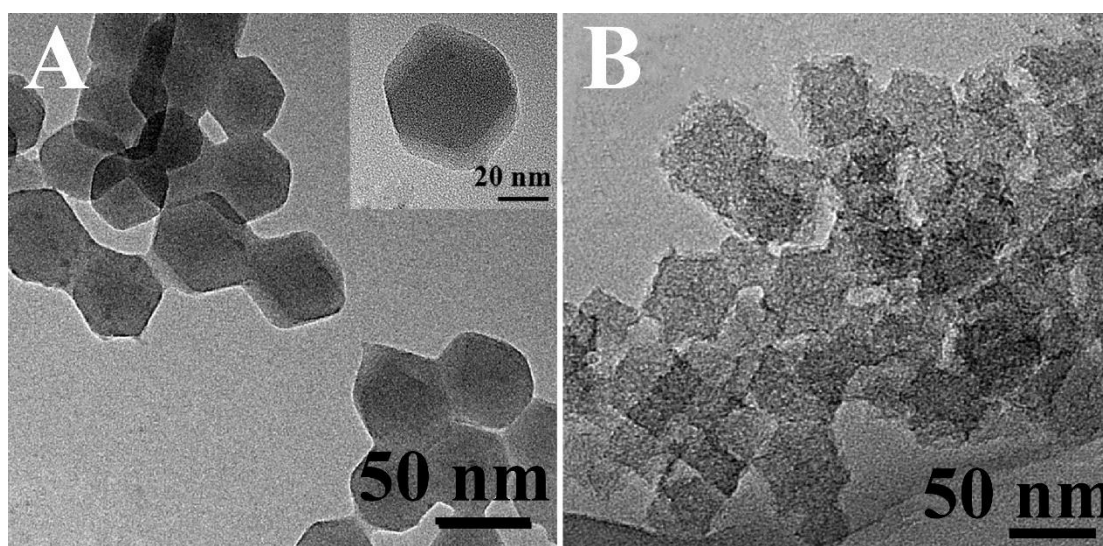


Figure 2. (A) TEM images of Ni²⁺-ZIF-8 and (B) TEM images of Ni@C

By studying the ray diffraction patterns of Ni@C, Ni²⁺-ZIF-8 and ZIF-8 (Fig. 3(A)), we found that the XRD patterns of Ni²⁺-ZIF-8 and ZIF-8 were almost identical, which proved that the Ni doping process did not change the crystal structure of ZIF-8 itself, which is consistent with the TEM results. At the same time, the spectrum of Ni@C shows two broad peaks at approximately 25° and 15°,

corresponding to the (002) and (111) diffraction peaks, respectively, which indicate the amorphous nature of the Ni@C synthesis. [19] In addition, Figure 3(B) shows the Raman spectra of Ni@C and carbonized ZIF-8 (ZI@C) in terms of the degree of graphitization of the materials. There are two distinct characteristic peaks, which are assigned to the D band and the G band of the carbon material. Data analysis showed that the I_D/I_G of ZIF-8 is 1.18, while the I_D/I_G of the target material Ni@C is 1.21, which explains the amorphous state of carbon in the Ni@C material. [20]

Figure 3(C) shows the nitrogen adsorption/desorption isotherms of the Ni@C and Ni²⁺-ZIF-8 materials. It can be concluded that the specific surface areas of the Ni²⁺-ZIF-8 and Ni@C materials are 765 m³ g⁻¹ and 1142 m³ g⁻¹, respectively. Ni@C has a large specific surface area of more than 1000 m²/g, which is due to the excellent structure of Ni-ZIF-8 and the ordered spatial pore structure. After calcination, the space becomes larger, which is conducive to sufficient mass transfer during the subsequent electrochemical sensor operation and provides space for the catalytic process.

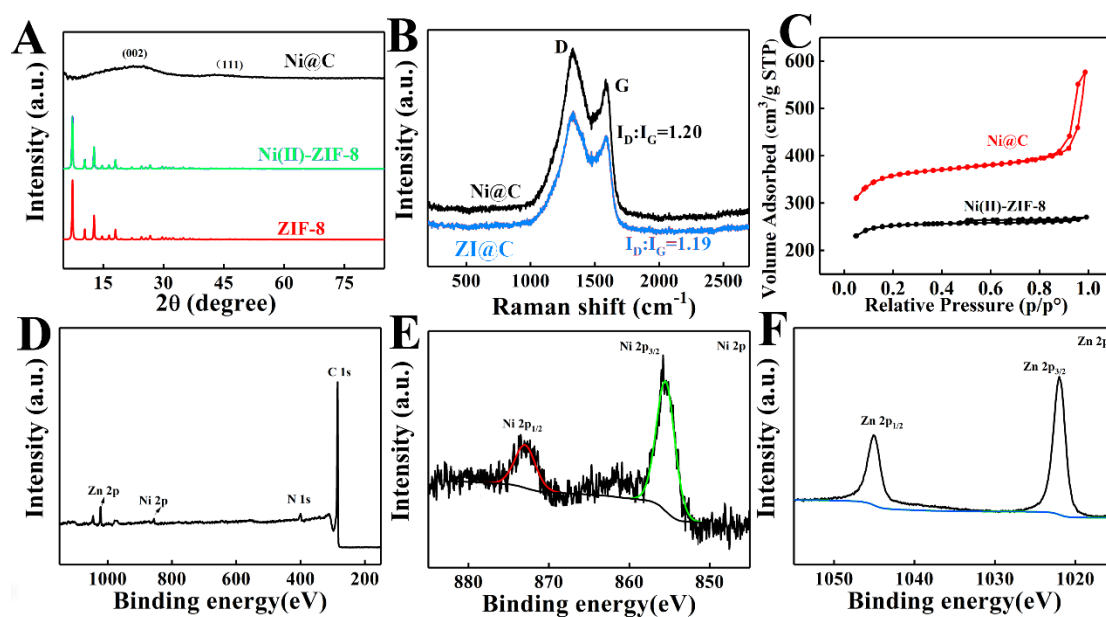


Figure 3. (A) XRD pattern of related materials; (B) Raman pattern; (C) N₂ adsorption pattern; (D) XPS spectrum; (E) XPS spectrum of Ni; (F) XPS spectrum of Zn.

X-ray photoelectron spectroscopy of the material was further performed to detect the presence of metal on the surface of Ni@C. Figure 3(D) shows the overall spectrum of the X-ray photoelectron spectrum of the material. Zn and Ni atoms are present in carbonized Ni@C. Figure 3(E) shows Ni peaks at 854.9 eV, 857.93 eV, 862.05 eV and 865.01 eV, which may be attributed to Ni 2p 2/3. Figure 3(F) also shows peaks at 1021.9 eV and 1045.6 eV corresponding to Zn 2p 3/2 and 2p 1/2, respectively, which are consistent with the previously reported results. [21-23] The above characterization results demonstrate the successful synthesis of Ni@C material.

3.2 Electrochemical characterization of Ni@C materials

Electrochemical impedance spectroscopy (EIS) was investigated, as shown in Fig. 4(A), to measure the Ni@C/GCE (curve a), bare GCE (curve b), and Ni²⁺-ZIF-8/GCE (curve c) charge transfer resistance (R_{ct}) values; the inset shows the Nyquist plot. By calculation, we can obtain R_{ct} values of 8.4, 48.1 and 32.2 Ωcm² for Ni@C/GCE (curve a), bare GCE (curve b), and Ni²⁺-ZIF-8/GCE (curve c)/GCE, respectively. The other materials have smaller electronic impedance than Ni²⁺-ZIF-8/GCE. This is because the organic framework structure of Ni²⁺-ZIF-8/GCE hinders the transport of electrons, while the synergistic effect of the three-dimensional carbon framework and Zn and Ni metal nanoparticles in the Ni@C material enhances the electronic conductivity. The regular hole structure of Ni@C is also favorable for the transport of [Fe(CN)₆]^{3-/4-}.

Furthermore, CV tests were performed with Ni@C/GCE, bare GCE Ni²⁺-ZIF-8/GCE and in 0.1 M KCl solution containing 5 mM [Fe(CN)₆]^{3-/4-}. As shown in Fig. 4(B), at a scan rate of 50 mV per second, the measured peak-to-peak potential difference (ΔE) values of Ni²⁺-ZIF-8/GCE, bare GCE, and Ni@C/GCE were 182, 132 and 123 mV, respectively. (Fig. 4B) These results are consistent with the EIS test, and the peak-to-peak potential difference of Ni@C/GCE is lower compared to the other materials, demonstrating the good redox behavior of ferricyanide ions at the modified electrode. This is attributed to the good electrical conductivity produced by the synergistic interaction of Ni with C and the abundant diffusion pathways provided by the large specific surface area and the corresponding fast electron/ion transport. The high electrical conductivity and fast electron transport suggest that Ni@C/GCE can be used for further electrochemical studies.

Translated with www.DeepL.com/Translator (free version)

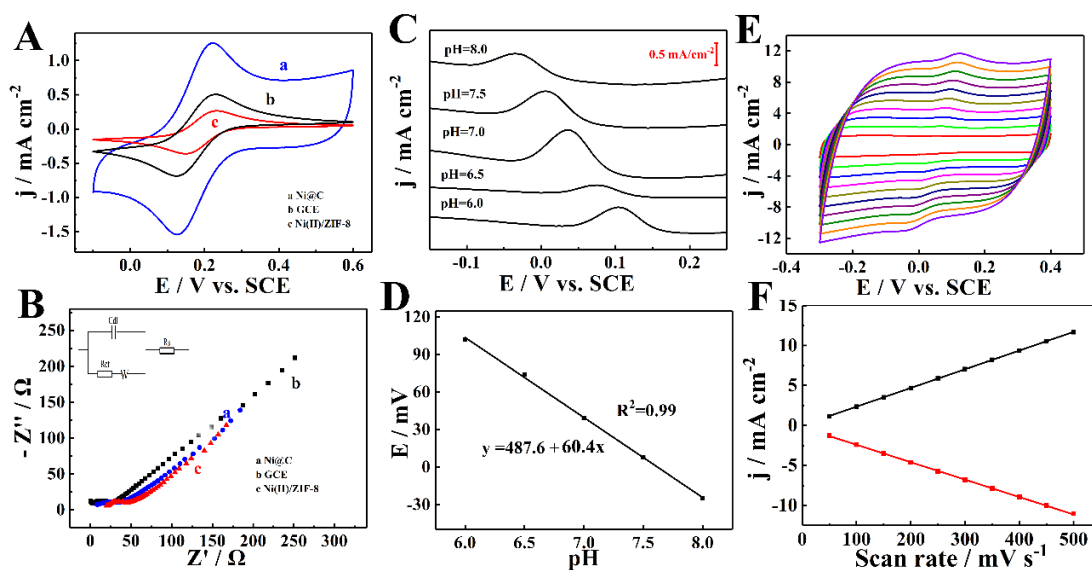


Figure 4. (A, B) CV plots and EIS of different electrodes in 0.1 M KCl aqueous solution containing 5 mM [Fe(CN)₆]^{3-/4-}. (C) DPV response of Ni@C/GCE in 0.2 M PBS with different pH values in addition to HQ. (D) Fitting curve between E_p and pH, (E) CV plots of the Ni@C/GCE in 0.2 M PBS at various scan rates in addition to HQ. (F) Plot of peak current density versus the scan rate.

DPV curves in the presence of HQ in nitrogen-saturated PBS solutions of different pH values (6.0 to 8.0) were then investigated. Figure 4(C) shows that the HQ peak potential gradually shifted negatively with increasing pH. Figure 4(D) shows the linear relationship between pH and E_{HQ} . The figure shows that pH and E_p have a very good linear relationship; the slope of the fitting curve in the figure is -60.4 mV/pH , which is close to the typical isoelectronic theoretical slope for the isoproton process of -59 mV/pH . [24,25]

To investigate the kinetic process of HQ catalyzed by the Ni@C/GCE electrode, CV maps of different scan rates in the presence of HQ in nitrogen-saturated 0.2 M PBS buffer solution (pH = 7.0) were plotted. Figure 4 (E) and (F) are the CV spectra and their linear fitting diagrams at different scan rates in the presence of HQ, respectively. As the scan rate increases, the redox peak current of HQ also increases. Figure 4(F) shows that the peak current density is proportional to the scan rate, revealing that the redox process of HQ on the Ni@C/GCE surface is a surface adsorption-controlled process.

To ensure the performance of the HQ sensor, a series of conditions are optimized based on Ni@C/GCE in this work. First, the coordination ratio of Zn^{2+} and Ni^{2+} was optimized, the sum of the contents of Zn and Ni was kept unchanged, and different Ni@C materials were synthesized by changing the ratio. As shown in Fig. 5(A), when the ratio of Zn/Ni is 5:1, the catalytic effect is the best. This may be because too little Zn causes the material to not crystallize normally, the structure collapses, the specific surface area decreases, and the metal falls off, resulting in a decrease in the catalytic ability. This directly leads to the reduction of catalytic capacity. Therefore, $\text{Zn}^{2+}/\text{Ni}^{2+}$ was chosen to be 5:1 for coordination. Subsequently, the pH value of the PBS solution was observed to show a crucial influence on the detection results. Therefore, we studied the HQ determination of the Ni@C/GCE electrode in 0.2 M PBS electrolyte solutions with different pH values, and the results are shown in Figure 5(B). When pH=7.0, the peak current density for detecting HQ reaches the maximum. Taking this into account, pH=7.0 was selected as the optimal detection pH value. Finally, the dropwise concentration of the Ni@C material on the GCE surface was optimized; Figure 5(C) shows the effect of different Ni@C concentrations on the final catalytic performance. When the concentration of Ni@C was lower than 2 mg/mL, the catalytic current of the material toward HQ gradually increased with increasing concentration. However, when the concentration of Ni@C was greater than 2 mg/mL, there were two factors to consider. On the one hand, GCE cannot stably fix a large number of materials, and Ni@C may fall into the electrolyte solution, resulting in the reduction of the catalytic current; on the other hand, the accumulation of materials may also hinder the transport of electrons, leading to a catalytic effect.

After optimizing a series of detection conditions, HQ was measured by differential pulse voltammetry using the Ni@C electrode, and the results are shown in Fig. 5(D). The oxidation peak of HQ appeared at approximately 0.03 V; at the same time, with the gradual increase in HQ concentration, the oxidation peak current density gradually increased. Through the linear fitting plot (Fig. 5(E)), we can determine that the sensitivity of the Ni@C electrochemical sensor to detect HQ alone is $180 \mu\text{A} \mu\text{M}^{-1} \text{cm}^{-2}$, and the linear range is 9.1 nM-80 μM . This result indicates that Ni@C can be effectively used as a catalytic material to construct electrochemical HQ sensors. The high sensitivity of the sensor is attributed to the efficient catalysis of Ni nanoparticles in the material, the strong electrical conductivity of the carbon skeleton, and the ordered structure of the material to facilitate the transfer of the detected species and electron conduction. Figure 5 (F) is the selectivity bar graph of HQ. In the presence of HQ,

other potential active interfering substances are added, including CC, RC, hydrogen peroxide, NaCl, KCl, ascorbic acid (AA), dopamine (DA) and sucrose. The changes caused by these interfering substances are all less than 10% of the current density, which is enough to prove that the sensor has good selectivity.

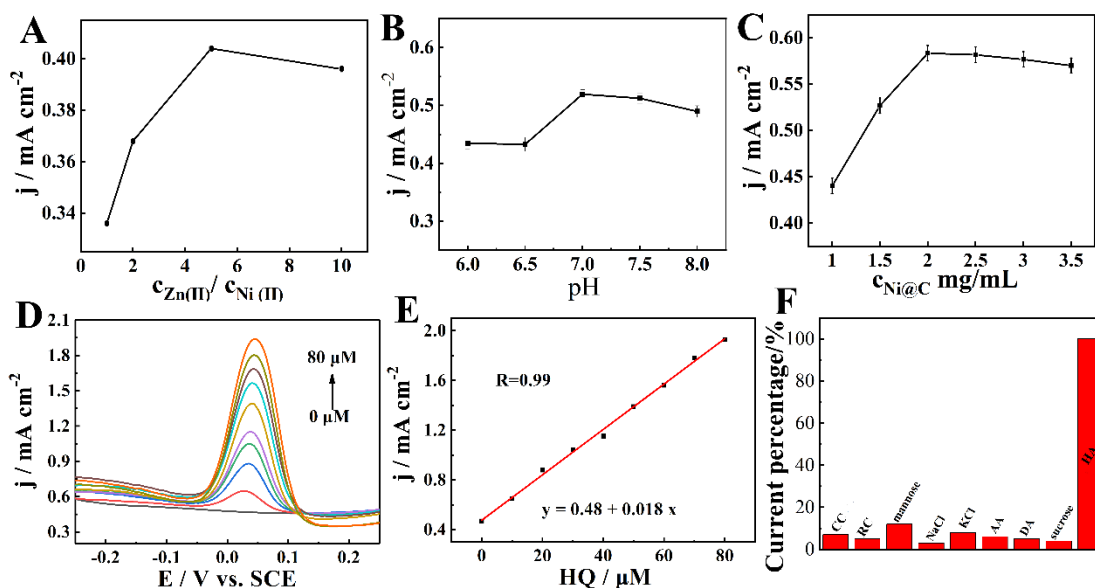


Figure 5. (A) Plot of the peak current density of HQ detected at the same ratio of Zn²⁺ to Ni²⁺. (B) Plot of the peak current density of HQ detected by Ni@C/GCE in different pH electrolyte solutions. (C) Plot of the peak current density of HQ detected by Ni@C/GCE with different concentrations. (D) The DPV of HQ detection by the Ni@C/GCE electrode. (E) The curve of the corresponding peak current density and concentration showing a linear relationship. (F) Interference histogram of some potential interfering substances in HQ detection

Table 1. Comparison of HQ electrochemical sensors. [26-32]

Modified Electrode	Linear range (μ M)	Detection limit (nM)	Reference
Ni@C/GCE	0.009-80 μ M	3.2	This work
Poly-L-Asn/GCE	3.3-40	224.7	[26]
Co ₃ O ₄ @C/GNPs/GCE	0.04–30	14	[27]
Cu-TCPP/GCE	0.01–12	3.4	[28]
CS/MWCNTs/PDA/AuNPs/GCE	0.1–10	3.5	[29]
WBC/Au/GCE	0.008–7.0	2	[30]
CMK - 3/GCE	1-30	100	[31]
PARS/CS/BCN -	1-100	190	[32]

Table 1 is a comparison table of the detection performance of different electrochemical sensors for HQ. The table shows that the Ni@C/GCE electrochemical sensor has a relatively wide linear range and a low detection limit. In this study, the excellent performance of the Ni@C/GCE sensor for detecting HQ is because the ZIF-8-derived porous carbon has a larger specific surface area, which makes it easier to enrich HQ. In addition, the Ni nanoparticles are highly conductive, so the composite prepared Ni@C shows a better performance than the individual components, has a larger specific surface area and strong electrical conductivity, and has better electrocatalytic activity for HQ. Therefore, the electrochemical sensor constructed in this study shows superior performance parameters.

In addition to detection performance, repeatability, reproducibility, and selectivity are also important features of a sensor. Therefore, the repeatability, reproducibility, and stability of the Ni@C-based sensor were explored. We used the Ni@C electrode for 30 days and continuously detected HQ. Within one month, the detection peak current density of HQ showed little change, and the relative standard deviation (RSD) was only 6.61%, indicating that the HQ sensor had good repeatability. At the same time, we selected ten Ni@C electrodes produced with the same synthesis steps to detect HQ under the same conditions, and the RSDs of HQ detected by the different electrodes were 5.32%, indicating that the Ni@C electrode has excellent reproducibility. The excellent repeatability and reproducibility of the sensor is related to the stable nature of Ni@C. The ordered internal structure of Ni@C provides sufficient space for the catalytic process of Ni while @C acts as protection and improves the stability of the material.

In addition, to evaluate the feasibility of Ni@C applications, the electrochemical sensing platform was used to perform spike recovery analysis experiments on local tap water samples. The samples were measured 3 times in parallel, and the RSD for these measurements was less than 5.0%. The recoveries ranged between 97.30% and 103.75%, as shown in Table 2, indicating that Ni@C/GCE can be used accurately and reliably for practical applications.

Table 2. Determination of HQ in tap water samples

Sample	Added (μM)	Found (μM)	Recovery (%)
Tap water samples	20.00	19.73	98.65
	40.00	41.5	103.75
	60.00	58.38	97.30

In conclusion, the HQ sensor based on Ni@C/GCE has good detection performance and performs well in terms of repeatability, reproducibility and selectivity. This indicates that Ni@C materials have potential for the construction of enzyme-free electrochemical sensors.

4. CONCLUSION

In summary, Ni-Zn-doped porous carbon materials (Ni@C) with regular dodecahedral morphology were synthesized by calcination of Ni-doped ZIF-8 as a template and applied in electrochemical sensing and quantitative electrochemical sensors to detect hydroquinone (HQ). The uniformly dispersed Ni in Ni@C serves as the catalytically active material, and the synergistic effect of elemental Zn and porous carbon improves the electron transport efficiency of the material. The results demonstrate that the enzyme-free electrochemical sensors based on Ni@C/GCE exhibit good sensitivity, a wide linear range and excellent selectivity. At the same time, the problem of the general conductivity of MOF materials is solved, which provides a new idea for the application of such new materials in the direction of electrochemistry.

ACKNOWLEDGMENT

This work was financially supported by the Science and Technology Research Project of Jiangxi Provincial Department of Education (GJJ218808)

References

1. Z. Xu, F. Liu, T. Zhang, Y. Gu, N. Lu, H. Xu, X. Yan, Y. Song, Y. Xing and D. Yu, *Anal. Chem.*, 92 (2020) 15297-15305.
2. A. R. Rajamani and S. C. Peter, *ACS Appl. Nano Mater.*, 1 (2018) 5148-5157.
3. H. Erikson, A. Sarapuu, J. Kozlova, L. Matisen, V. Sammelselg and K. Tammeveski, *Electrocatalysis*, 6 (2015) 77-85.
4. L. Wang, C. Gong, Y. Shen, M. Xu, G. He, L. Wang and Y. Song, *Sens. Actuators, B*, 265 (2018) 227-233.
5. Y. Wu, L. Jiao, X. Luo, W. Xu, X. Wei, H. Wang, H. Yan, W. Gu, B. Z. Xu and D. Du, *Small*, 15 (2019) 1903108.
6. C. Baldizzone, S. Mezzavilla, H. W. Carvalho, J. C. Meier, A. K. Schuppert, M. Heggen, C. Galeano, J. D. Grunwaldt, F. Schüth and K. J. Mayrhofer, *Angew. Chem. Int. Ed.*, 53 (2014) 14250-14254.
7. G.-H. Wang, J. Hilgert, F. H. Richter, F. Wang, H.-J. Bongard, B. Spliethoff, C. Weidenthaler and F. Schüth, *Nat. Mater.*, 13 (2014) 293-300.
8. L. Zhang, Z. Liu, Q. Deng, Y. Sang, K. Dong, J. Ren and X. Qu, *Angew. Chem. Int. Ed.*, 60 (2021) 3469-3474.
9. Y. Zhu, W. D. Wang, X. Sun, M. Fan, X. Hu and Z. Dong, *ACS Appl. Mater. Interfaces*, 12 (2020) 7285-7294.
10. D. J. Bell, M. Wiese, A. A. Schönberger and M. Wessling, *Angew. Chem.*, 132 (2020) 16181-16187.
11. I. M. Hönicke, I. Senkovska, V. Bon, I. A. Baburin, N. Bönisch, S. Raschke, J. D. Evans and S. Kaskel, *Angew. Chem., Int. Ed.*, 57 (2018) 13780-13783.
12. J. H. Cavka, S. Jakobsen, U. Olsbye, N. Guillou, C. Lamberti, S. Bordiga and K. P. Lillerud, *J. Am. Chem. Soc.*, 130 (2008) 13850-13851.
13. W.-J. Shen, Y. Zhuo, Y.-Q. Chai and R. Yuan, *Anal. Chem.*, 87 (2015) 11345-11352.
14. X. Fang, X. Chen, Y. Liu, Q. Li, Z. Zeng, T. Maiyalagan and S. Mao, *ACS Appl. Nano Mater.*, 2 (2019) 2367-2376.
15. H. He, S. Lv, Y. Kang, J. Yi, Y. Zhang and Y. Cong, *J. Electroanal. Chem.*, (2022) 116540.

16. T. Anandhu, R. R. Mohan, J. Cherusseri, R. Rohith and S. J. Varma, *Electrochim. Acta*, (2022) 140740.
17. J. Nordlund, P. Grimes and J. P. Ortonne, *J. Eur. Acad. Dermatol.*, 20 (2006) 781-787.
18. D. McGregor, *Crit. Rev. Toxicol.*, 37 (2007) 887-914.
19. Y. Zhang, L. Gomez, F. N. Ishikawa, A. Madaria, K. Ryu, C. Wang, A. Badmaev and C. Zhou, *J. Phys. Chem. Lett.*, 1 (2010) 3101-3107.
20. S. Zhang, X. Zeng, H. Xie and P. Hing, *Surf. Coat. Technol.*, 123 (2000) 256-260.
21. A. Naghash, T. Etsell and S. Xu, *Chem. Mater.*, 18 (2006) 2480-2488.
22. H. Nesbitt, D. Legrand and G. Bancroft, *Phys. Chem. Miner.*, 27 (2000) 357-366.
23. A. P. Grosvenor, M. C. Biesinger, R. S. C. Smart and N. S. McIntyre, *Surf. Sci.*, 600 (2006) 1771-1779.
24. M. Lian, Y. Shi, W. Zhang, J. Zhao and D. Chen, *J. Electroanal. Chem.*, 904 (2022) 115849.
25. S. Hu, H. Chen, X. Zhan, X. Qin, Y. Kuang, M. Li, Z. Liang, J. Yang and Z. Su, *J. Electroanal. Chem.*, 897 (2021) 115590.
26. Y. Lu, R. Jin, Y. Qiao, J. Liu, X. Wang, K. Wang and C. Wang, *Int. J. Electrochem. Sci.*, 14 (2019) 10043-10057.
27. M. F. Pistonesi, M. S. Di Nezio, M. E. Centurión, M. E. Palomeque, A. G. Lista and B. S. F. Band, *Talanta*, 69 (2006) 1265-1268.
28. J. Tashkhourian, M. Daneshi, F. Nami-Ana, M. Behbahani and A. Bagheri, *J. Hazard. Mater.*, 318 (2016) 117-124.
29. L. Ji, Q. Wang, L. Peng, X. Li, X. Zhu and P. Hu, *Materials*, 15 (2022) 4625.
30. X. Yang, C. He, Y. Lin, Y. Qiu, P. Li, Y. Chen, B. Huang and X. Zheng, *Anal. Methods*, 14 (2022) 34-43.
31. J. Yu, W. Du, F. Zhao and B. Zeng, *Electrochim. Acta*, 54 (2009) 984-988.
32. J. Qu, Y. Wang, J. Guo, Y. Dong and T. Lou, *J. Electrochem. Soc.*, 161 (2014) B220.